Quantitative high-resolution 7T MRI to assess longitudinal changes in articular cartilage after anterior cruciate ligament injury in a rabbit model of post-traumatic osteoarthritis

Osteoarthritis and Cartilage Open 4 (2022) 100259

Contents lists available at ScienceDirect

Osteoarthritis and Cartilage Open

journal homepage: www.elsevier.com/journals/osteoarthritis-and-cartilage-open/2665-9131

Quantitative high-resolution 7T MRI to assess longitudinal changes in articular cartilage after anterior cruciate ligament injury in a rabbit model of post-traumatic osteoarthritis

Rossana Terracciano [a,b], Yareli Carcamo-Bahena [a], Amber Lee R. Royal [a], Danilo Demarchi [b], John Scott Labis [c], Joshua D. Harris [d], Bradley K. Weiner [d], Nakul Gupta [c], Carly S. Filgueira [a,e,*]

[a] Department of Nanomedicine, Houston Methodist Research Institute, Houston, TX, 77030, USA
[b] Department of Electronics, Politecnico di Torino, Torino, Italy
[c] Department of Radiology, Houston Methodist Hospital, Houston, TX, 77030, USA
[d] Department of Orthopedic Surgery, Houston Methodist Hospital, Houston, TX, 77030, USA
[e] Department of Cardiovascular Surgery, Houston Methodist Research Institute, Houston, TX, 77030, USA

ARTICLE INFO

Keywords:
Post-traumatic osteoarthritis
Ultra-high field MRI
dGEMRIC
Micro-computed tomography
Osteophytes
Histology

ABSTRACT

Objective: To demonstrate an ultra-high field (UHF) 7 T delayed gadolinium-enhanced MRI of cartilage (dGEMRIC) protocol for quantitative post-traumatic osteoarthritis (PTOA) detection and monitoring in a rabbit anterior cruciate ligament transection (ACLT) model.

Design: ACL transections were performed unilaterally in 5 rabbits (33-weeks-old, 3.5 ± 0.5 kg) to induce PTOA. MRI exams were performed at 7 T prior to and 2, 4, 7 and 10-weeks after ACLT using a modified dGEMRIC protocol. Voxel-based T1 and T2 maps were created over manually drawn femoral cartilage ROIs from the center of the tibial plateau to the posterior meniscus. Femoral, tibial, and patellar epiphyses were harvested 10-weeks post-surgery and processed for μCT imaging and histology.

Results: Quantitative analysis revealed a 35% and 39% decrease in dGEMRIC index in the medial ACLT knee compartment 7- and 10-weeks post-surgery, respectively ($p = 0.009$ and $p = 0.006$) when compared to baseline. There was no significant change in the lateral ACLT compartment or in either compartment of the control knees. Visual inspection of histology confirmed PTOA in the ACLT knees. Osteophytes were found only in ACLT knees (osteophyte volume in femur: 94.53 ± 44.08 mm^3, tibia: 29.35 ± 13.79 mm^3, and patella: 3.84 ± 0.92 mm^3) and were significantly larger in the medial compartments of the femur than lateral ($p = 0.0312$).

Conclusion: The dGEMRIC technique quantitatively applied at 7 T UHF-MRI demonstrates site-specific cartilage degeneration in a large animal PTOA model. This should encourage further investigation, with potential applications in drug and therapeutic animal trials as well as human studies.

1. Introduction

Post-traumatic osteoarthritis (PTOA), a subset of osteoarthritis (OA), develops from acute or repetitive joint injury and accounts for an estimated 12% of all OA cases [1]. Direct costs for treating PTOA exceed $3 billion annually in the United States alone [2]. The time course of PTOA is highly variable and breakdown of articular cartilage can occur early on or years after initial injury [3–5]. In the early acute post-traumatic phase, also known as the clinically asymptomatic period, biochemical modifications such as metabolic changes occur in the articular cartilage. Mechanical damage also leads to changes in gene expression and cartilage metabolism which result in morphological changes such as articular cartilage thinning and degradation. These early articular cartilage changes are not visible in routine radiographs [6], which are only able to detect gross osseous alterations that occur late in the disease [7].

Since PTOA is a complex and dynamic process, animal models are essential to understand the disease and assess therapeutic interventions. Large animal models are advantageous as their anatomy is markedly similar to humans and they have thicker cartilage than small animal models, such that imaging can be performed using clinical instrumentation allowing for easier human translation. Although the cartilage in rabbits is 5–10x thinner compared with humans [8], rabbit models offer

* Corresponding author. Department of Nanomedicine, Houston Methodist Research Institute, Houston, TX, 77030, USA.
E-mail address: csfilgueira@houstonmethodist.org (C.S. Filgueira).

https://doi.org/10.1016/j.ocarto.2022.100259
Received 8 November 2021; Received in revised form 28 February 2022; Accepted 30 March 2022

advantages over other larger animal models, including a slower growth curve, maintaining similar size during a longitudinal study. Rabbits in particular have also served as reproducible models to study PTOA, and ACL transection is a common means for surgical induction [9]. Although ACL injury is well-recognized, it is an under-researched risk factor for developing knee PTOA due to chronic instability.

Currently, there is no effective treatment for PTOA and non-invasive methods to assess its progression remain a largely unmet clinical need [4,5,10]. In order to develop effective therapeutics, it is critical to have non-invasive methods for early PTOA detection and disease progression monitoring [11]. Several studies report that initial biochemical changes of cartilage degeneration following ACL tear involve disruption of the collagen network [12], decrease in proteoglycan (glycosaminoglycan, GAG) content [13,14], and increase in permeability to water [15]. In addition to these changes in articular cartilage, alterations in femoral and tibial subchondral bone micro-architecture have been recorded in rabbits after ACLT. Sulaiman et al. revealed a bone remodeling processes of ACLT rabbit knees after 8–12 weeks, with an increase in subchondral bone volume, thickening of trabeculae, reduced trabecular separation, and reduced porosity, due to redistribution of forces and adaptation after the traumatic event [16].

Compositional MRI techniques allow for biochemical marker detection of functional and structural cartilage integrity before morphological changes occur [17]. One of the most well-established compositional MRI methods for early cartilage quality assessment in OA is delayed Gadolinium Enhanced Magnetic Resonance Imaging of Cartilage (dGEMRIC) [18,19]. A standard dGEMRIC protocol allows T1 relaxation-time measurements using the negative ionic charge of an intravenously injected gadolinium-based contrast agent, which distributes into articular cartilage in a spatially inverse relationship to the concentration of negatively charged GAG molecules [20]. Water content and 3D architecture of collagen within cartilage can be instead evaluated using the transverse spin relaxation-time constant (T2) [21].

While the dGEMRIC approach is proven to sensitively detect early cartilage degeneration at clinical MRI field strengths [17,22,23], few studies involving human subjects have been conducted with ultrahigh-field MRI (UHF-MRI) [24,25]. UHF-MRI at 7 T allows for superior SNR compared to clinical 1.5 T or 3 T, which can be leveraged to enhance spatial resolution and/or reduce imaging time. To our knowledge, no longitudinal dGEMRIC studies involving ACLT rabbits have been conducted with 7 T to quantitatively assess PTOA progression. Such a study could pave the way for testing biologics and devices in clinical studies as interventions in PTOA. The purpose of this work is to demonstrate feasibility of a 7 T MRI dGEMRIC protocol in an ACLT rabbit model to longitudinally monitor and quantify disease evolution and confirm site-specific degeneration induced by early PTOA using 3D high-resolution μCT.

2. Methods

2.1. Animal model

The study was performed between March 2021 and June 2021. All animal procedures were approved by the Institutional Animal Care and Use Committee (IACUC) at Houston Methodist Research Institute (IACUC # IS00005825). Five female New Zealand White rabbits 33-weeks-old and 3.5 ± 0.5 kg (Envigo Corp., Indianapolis, Ind) were studied. With 5 subjects, our study had 80% power at alpha = 0.05 to detect a 25% drop in T1 time/dGEMRIC index and is similar to prior studies such as Wachsmuth et al. [26] which used three subjects per time point to evaluate the rabbit knee with μMR and Wei et al. [27] which used four subjects per time point to analyze the porcine knee with T1 time/-dGEMRIC index. Digital radiography was performed using an XRpad 4336 MED digital x-ray detector system on a Minxray HF120/60HPPWV Power Plus prior to surgery to confirm skeletal maturity (Fig. E2). ACL transection (Figure E1) was performed following protocols outlined by Sieker et al. [28] and Vavken et al. [29] in the right stifle joint, equivalent to the human knee and often the largest synovial joint in the animal's body. Left knees were used as a contralateral control group. Females were chosen as they reach skeletal maturity earlier [30] and female humans are two-to-ten times more likely to experience ACL injury [31] and present in more advanced stages of OA with more debilitating knee pain than males [32]. This model eliminates inconsistency in age, weight, genetics, and environmental conditions to reduce variability of clinical manifestation of the disease. Animal weights were grossly stable over the longitudinal study, although there was a decrease 2-weeks post-surgery due to the ACL surgical procedure with subsequent recovery (Fig. E3).

2.2. Animal preparation

Gadobenate dimeglumine (Gd-BOPTA, MultiHance; 529 mg/mL, Bracco Diagnostics Inc., Monroe Twp., NJ) was administered as a bolus injection (0.5 mL/kg) in the rabbit lateral ear vein similar to the protocol described by Wachsmuth et al. [26], and the rabbits were permitted to ambulate for 10 min in a free space. The ambulation process was overseen by three investigators (R.T., Y.C.B., A.L.R.R.) to ensure that contrast was fully diffused into the joint cartilage. Animal sedation occurred via intramuscular injection of a cocktail solution of 50 mg/kg ketamine and 1 mg/kg midazolam into the epaxial lumbar muscles to avoid any confounding signal abnormalities due to intramuscular injury/edema from sedation. Animals were intubated and maintained with isoflurane via mechanical ventilation and monitored for various physiologic parameters using the Invivo Expression MRI monitoring system. Pre-contrast T1 (native T1pre) and T2 images were acquired 2 weeks prior to ACL surgery. Native T1pre was assessed only once at the beginning of the study to minimize sedation events and associated risks. Post-contrast T1 images for dGEMRIC index (T1Gd) were acquired 1 week before surgery and compared with native T1pre images to account for possible variations in intensity and Gd uptake across the different joints. Follow-up T1Gd imaging occurred 2, 4, 7, and 10 weeks after surgery. The delay between intravenous administration of the contrast and start of the MR examination was kept at 60 ± 10 min to allow for complete penetration of Gd-BOPTA into the cartilage. While this delay is typically kept at 90 min in humans, it was previously demonstrated that T1 does not change significantly in dGEMRIC protocols when comparing results obtained using 60 and 90 min delay [33]. Additionally, rabbit body size and circulation result in faster contrast distribution compared to humans, such that shorter time delay is needed for post-contrast imaging [26]. Therefore, we set this parameter at 60 min to minimize sedation time.

2.3. Image acquisition

MR images were acquired with a MAGNETOM Terra 7 T MRI scanner (Siemens Medical Solutions USA Inc., Malvern, PA) using a commercially available 1Tx/28Rx human knee coil (Quality Electrodynamics, Mayfield Village, OH). Rabbits were laterally positioned with both knee joints centrally placed in the coil for simultaneous imaging. The coil was placed isocenter to the MR unit. A B1 field mapping sequence was performed for B1 field inhomogeneity correction (repetition time 23060.0 ms; flip angle 8°; bandwidth 490 Hz/pixel; field of view 160 mm; voxel size 2.5 × 2.5 × 1.5 mm^3; number of slices 60; number of signals acquired one; total acquisition time 0:48 min). For pre- and post-contrast T1 analysis of articular cartilage, a 3D Flash variable flip angle pulse sequence (repetition time 13 ms; echo time 5.19 ms; flip angles 4°, 15°; bandwidth 270 Hz/pixel; field of view 160 mm; voxel size 0.1 × 0.1 × 1.5 mm^3; number of slices 60; number of signals acquired 3; total acquisition time 21:54 min, water excitation on) was used. T2 mapping was performed with a spin echo sequence (echo times 11.1, 22.2, 33.3, 44.4 ms, repetition time 3080 ms; flip angle 180°; bandwidth 417 Hz/pixel; field of view 160 mm; voxel size 0.2 × 0.2 × 1.5 mm^3; number of slices 16; number of signals acquired 3; total acquisition time 12:52 min). Sagittal acquisitions were chosen to maintain the cartilage imaging assessment in an orientation

orthogonal to the weight-bearing aspects of the femoral condyles, tibial plateau, and patellar cartilage. Water excitation was chosen to selectively excite protons not bound to fat, resulting in shorter scan time and minimizing chemical shift artifacts [34]. To avoid variability due to scan-rescan we used a MR-SPOT skin marker (Beekley Medical) on the rabbit's right knee to ensure imaging the same region throughout the follow-up period.

2.4. Image analysis

Quantitative image analysis was performed by one researcher (R.T.) in consensus with a board-certified radiologist (N.G., 6 years of experience in MR imaging). Voxel-based T1 maps were calculated following the approach by Lee et al. [35]. dGEMRIC index was quantified in the lateral and medial femoral cartilage for both ACLT and control knees. Segmentation was manually performed for cartilage evaluation in 2–3 adjacent slices. ROIs covered the whole depth (up to 5 pixels) of the femoral cartilage ranging from the center of the tibial plateau to the posterior boundary of the respective medial or lateral meniscus. Gadolinium uptake in femoral cartilage was calculated for all pre-surgical images as the ratio between relaxation rate (defined as $\Delta R1 = 1/T1Gd\text{-}1/T1pre$ where T1pre and T1Gd corresponds to cartilage pre- and post-contrast value, respectively) and T1 relaxivity of Gd-BOPTA at 7 T (calculated by Shen et al. [36] as 4.67 s^{-1} mM^{-1}). T2 maps were obtained in-line using a pixel-wise, non-negative, mono-exponential curve fitting with Levenberg-Marquardt nonlinear least squares algorithm (*fittype*) discarding the first echo, following Milford et al. [37]. ROI analyses were manually performed for evaluation on the first echo set of images, with the same approach described for the dGEMRIC index. All custom written scripts are available online (https://github.com/rterracciano/dGEMRIC-MRI-Data-Analysis.git). ROIs in the MRI analysis were co-localized with histology images as explained in the following sections.

2.5. Osteophyte quantification

10 weeks post-surgery, the animals were euthanized, and the knee joints harvested. The tibia and femur were further transected at the level of the physis. High-resolution μCT images of *ex vivo* samples were acquired using a Siemens Inveon Preclinical Multimodality SPET/PET/CT System (80 kVp tube potential, 500 μA current, and 270 ms exposure time) along with Inveon acquisition workplace software (Siemens, Erlangen, Germany). Reconstructed image slices were 512 × 512 pixels in the axial plane, resulting in an isotropic nominal resolution of 40 μm. To quantify osteophyte volume, a 3D image registration was applied to the μCT images, co-aligning ACLT bones to their contralateral control, and subtraction images were used to measure volumetric differences between pairs of femurs, tibiae, and patellae, due to osteophytes (Figure E5). All μCT analysis, including determination of mean osteophyte volume and standard error were performed with 3DSlicer (https://www.slicer.org/).

2.6. Histologic sample preparation and examination

Samples were fixed in 10% neutral buffered formalin (NBF, StatLab Medical Products, Brooklyn, NY) for 24 h and decalcified with Formical-4 (StatLab Medical Products, Brooklyn, NY) for 15–20 days until decalcification endpoint. Paraffin blocks were sliced at 4 μm and stained with Safranin O-Fast Green (Sigma-Aldrich, St. Louis, MO, HT90432, F-7252) in the sagittal plane to evaluate distribution of proteoglycans in the cartilage. Slides were imaged (20x) using an EVOS FL Auto microscope (Life Technologies, Carlsbad, CA). Histological focus was kept consistent with the ROI analyzed at UHF-MRI. Histological grading was scored following Laverty et al. standards [38].

2.7. Statistical analysis

Data presented in all bar graphs are reported as mean ± standard error of the mean. Data presented in all box and whiskers graphs show a line plotted in the middle of the box as the median and whiskers as min and max values. Only data normally distributed were included in the results. Multiple unpaired t tests were used to compare Gd uptake in the medial and lateral femoral cartilage between the operated and contralateral knee joints. Two-way analysis of variance and Tukey's post hoc test for multiple comparisons were used to compare: 1) baseline with each post-surgery imaging timepoint after Gd administration for both dGEMRIC index and T2 mapping; 2) medial and lateral osteophyte volumes measured in the femur, tibia, and patella; 3) medial and lateral histologic grading scores in the femur. One-way analysis of variance and Tukey's post hoc test for multiple comparisons were used to compare the ratio between total osteophyte volume and total ACLT bone volume in the femurs, tibiae, and patellae. For all performed tests, p values less than 0.05 were considered statistically significant. Statistical analyses were conducted using GraphPad software (GraphPad Prism version 9.1.1; GraphPad Software, Inc., San Diego, Calif).

3. Results

3.1. dGEMRIC index

There was no statistically significant difference in Gd uptake between right and left knees at baseline ($p = 0.06$) (Fig. 1). However, after ACL transection, there was progressive T1 shortening compatible with declining GAG concentrations in the medial femoral cartilage of the injured knee when compared with the contralateral (uninjured) knee. The average native T1 pre-surgical values in the medial compartment of the femoral cartilage were 1128.94 ± 164.78 ms for the right knee and 1214.87 ± 114.89 ms for the left knee. For the ACLT knees, a significant difference was found between T1Gd baseline (pre-injury) and 7 weeks post-injury ($p = 0.01$) with 35% decrease ($T1Gd_{7w} = 299.64 \pm 40.49$ ms versus $T1Gd_{baseline} = 463.76 \pm 39.60$ ms), as well as 10 weeks post-injury ($p = 0.01$), where there was a 39% decline compared to the baseline ($T1Gd_{10w} = 282.76 \pm 24.76$ ms versus $T1Gd_{baseline} = 463.76 \pm 39.60$ ms). No significant differences were observed among the timepoints in the contralateral uninjured control knee. No significant differences were found between the injured (right) and control (left) knees for Gd uptake in lateral femoral cartilage ($p = 0.10$) at baseline, nor were there statistically significant differences between timepoints (Fig. 2). The average native T1 pre-surgery values in the lateral compartment of the femoral cartilage were 1071.98 ± 123.76 ms and 1220.79 ± 47.30 ms in the right and left knees, respectively. We also did not find significant differences between the injured (right) and control (left) knees for T1Gd in the medial or lateral tibial cartilage (Fig. E4).

3.2. T2 mapping

No significant differences between timepoints in the T2 mapping of the medial (Fig. 3) or lateral (Fig. 4) femoral cartilage were identified for both ACLT and control knees.

3.3. Histopathology

Post-mortem gross specimens of the medial femoral cartilage (Fig. 5a and b) demonstrated surface irregularities, cracking, and full-thickness ulceration at 10 weeks in the injured knee, which were absent in the contralateral knee. Notably, histochemical stains performed with Safranin O-Fast Green demonstrated greater degeneration in the medial compartment of the femoral cartilage than the lateral (Fig. 5c–f). Grading scores revealed structural/cellular organization and intensity differences between groups (Fig. 5g and h). In the ROI, ACLT cartilage degeneration was characterized by reduced staining intensity, increased surface

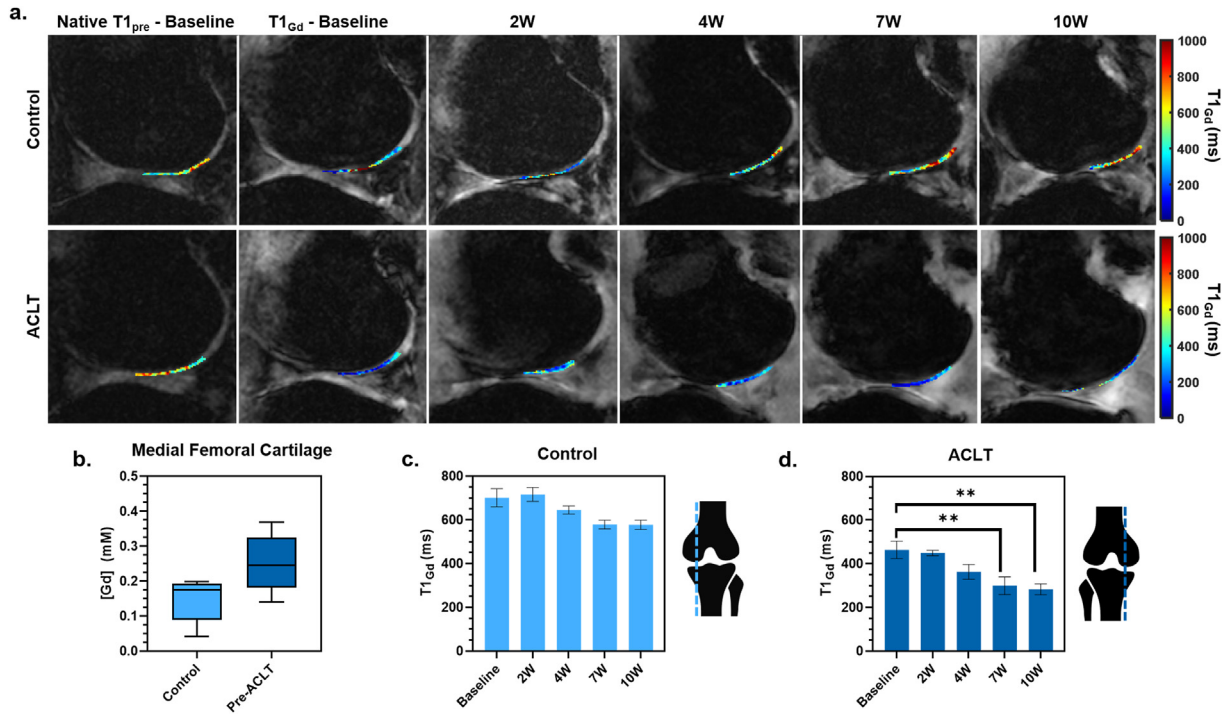

Fig. 1. dGEMRIC index (T1Gd) in the medial femoral cartilage for both ACLT and control knees. (a) Mid-sagittal slice T1Gd map overlaid on 3D Flash VFA. (b) Gadolinium uptake in the medial femoral cartilage compared between the contralateral (control) group and the ACLT pre-surgery group. dGEMRIC index in the medial compartment of the femoral cartilage for the (c) contralateral healthy control and (d) ACLT group. * = significant difference between baseline (no injury) and number of weeks after ACLT.

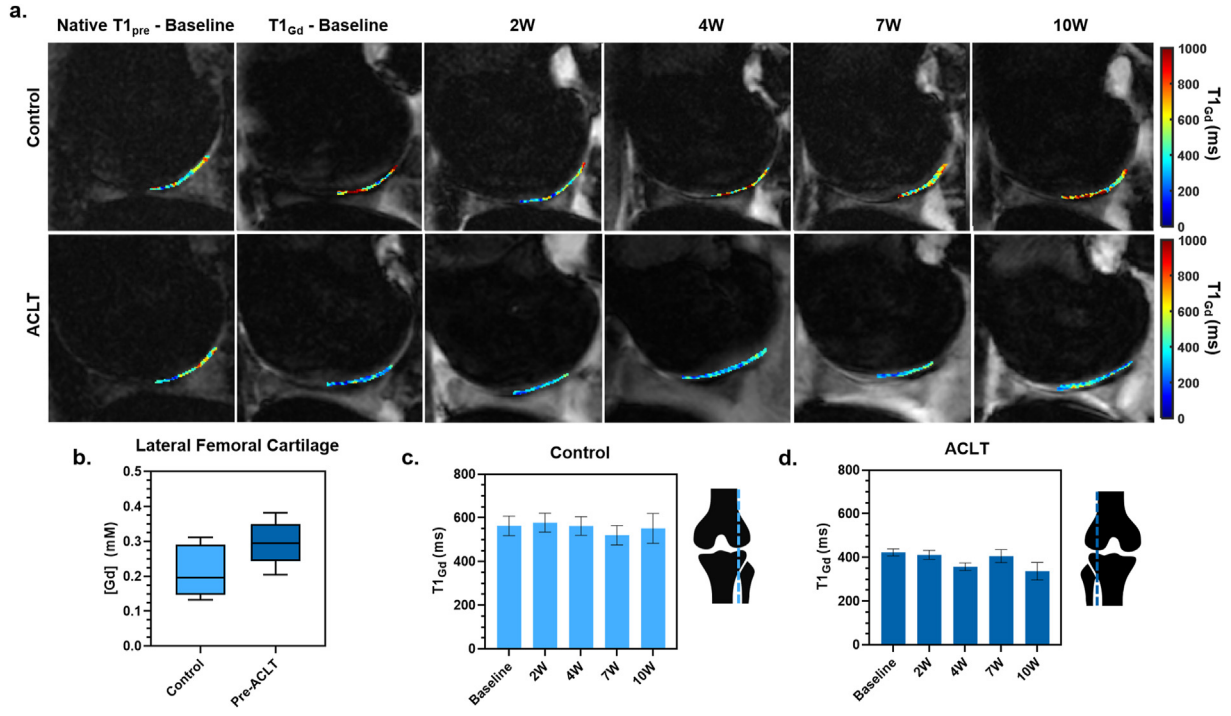

Fig. 2. dGEMRIC index (T1Gd) in the lateral femoral cartilage for both ACLT and control knees. (a.) Mid-sagittal T1Gd map overlaid on 3D Flash VFA. (b.) Gadolinium uptake in the lateral femoral cartilage for both the contralateral control group and the pre-surgery ACLT group. dGEMRIC index in the lateral compartment of femoral cartilage shown for the (c.) contralateral healthy control and (d.) ACLT groups. No significant difference between groups was found.

irregularities and erosion, and gradual gathering and reorganization of chondrocytes, including cluster formation and increased chondrocyte density, indicating decreased GAG content in the co-localized ROI, confirming the 7 T quantifications (Fig. E6).

3.4. *μCT obtained osteophyte volumes*

μCT images of *ex vivo* femur, tibia, and patella bones demonstrate osteophytes at the ACLT joint margins most notably in the femur medial

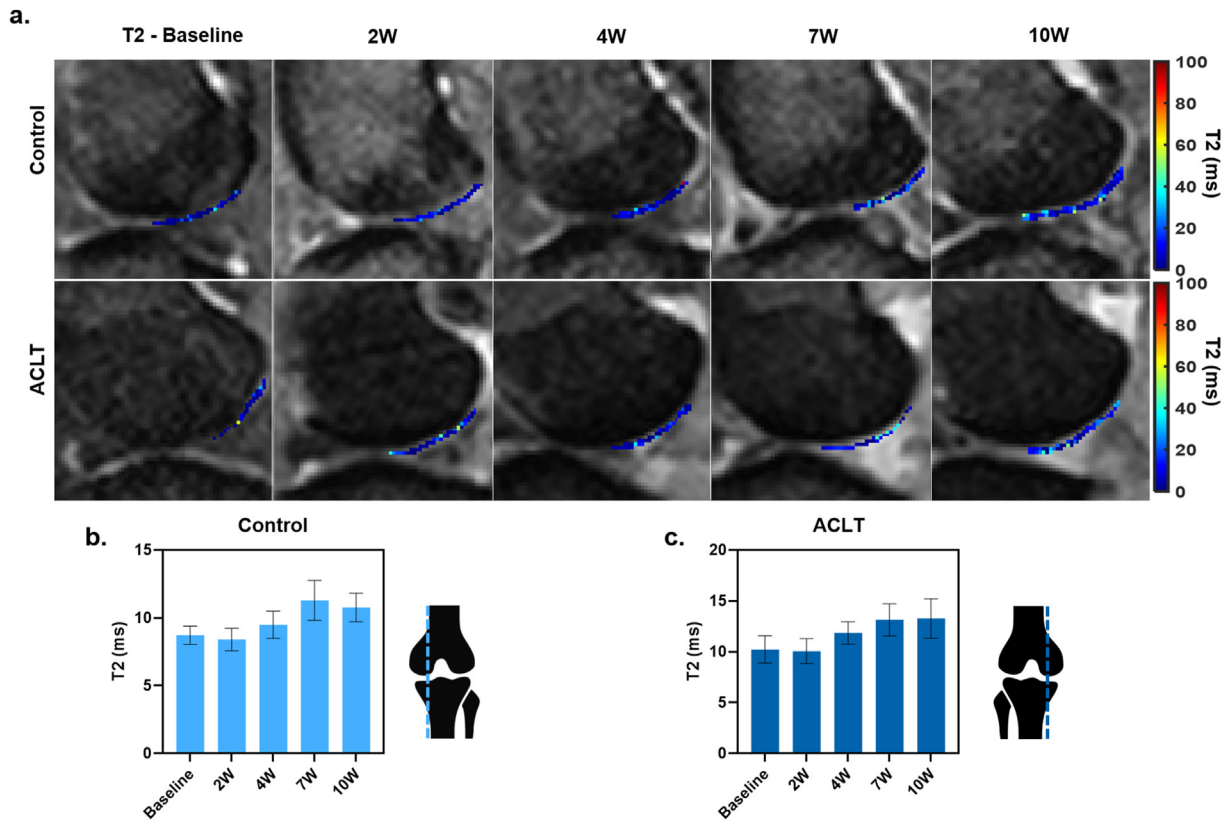

Fig. 3. T2 in the medial femoral cartilage for both ACLT and control knees. (a.) Mid-sagittal T2 map overlaid on the first echo acquired with a Spin Echo sequence. T2 in the medial compartment of femoral cartilage for the (b.) contralateral healthy control and (c.) ACLT group demonstrates no significant change.

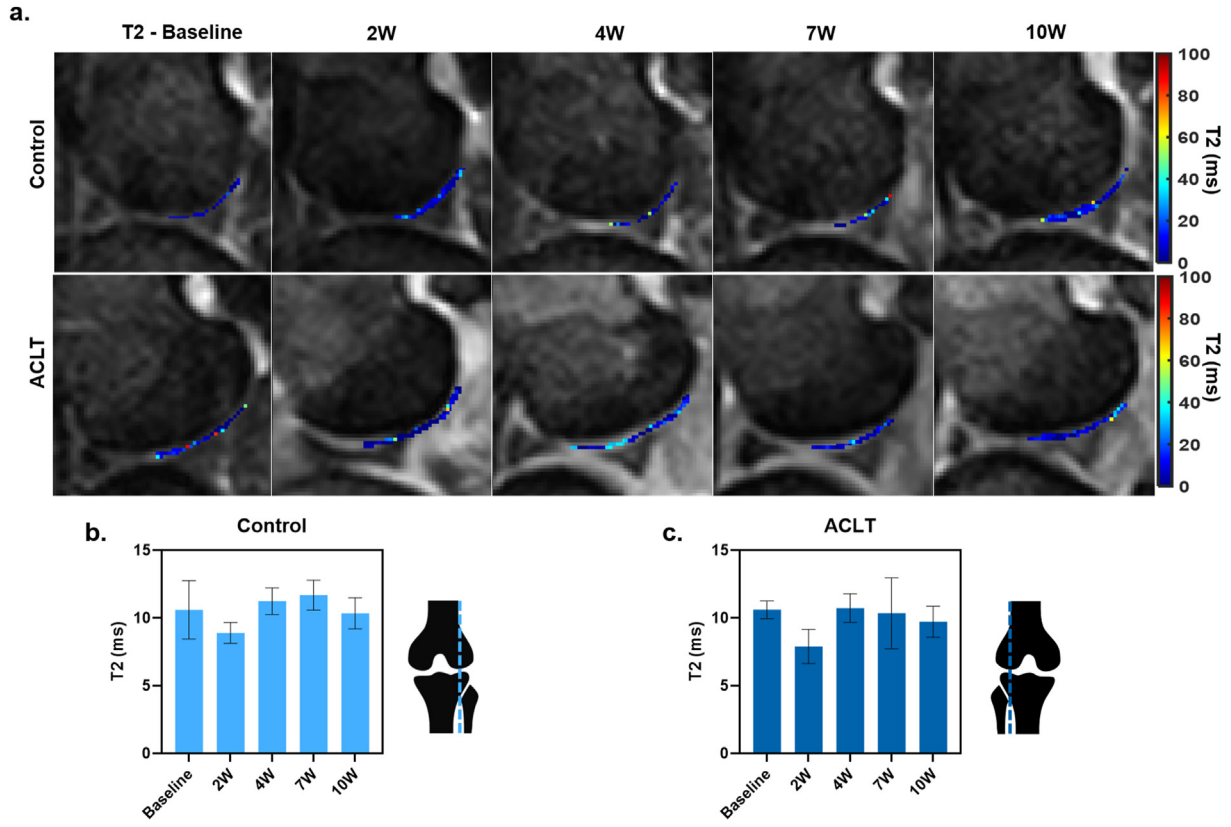

Fig. 4. T2 in the lateral femoral cartilage for both ACLT and control knees. (a.) Mid-sagittal T2 map overlaid on the first echo acquired with a Spin Echo sequence. T2 in the medial compartment of femoral cartilage for the (b.) contralateral healthy control and (c.) ACLT group demonstrates no significant change.

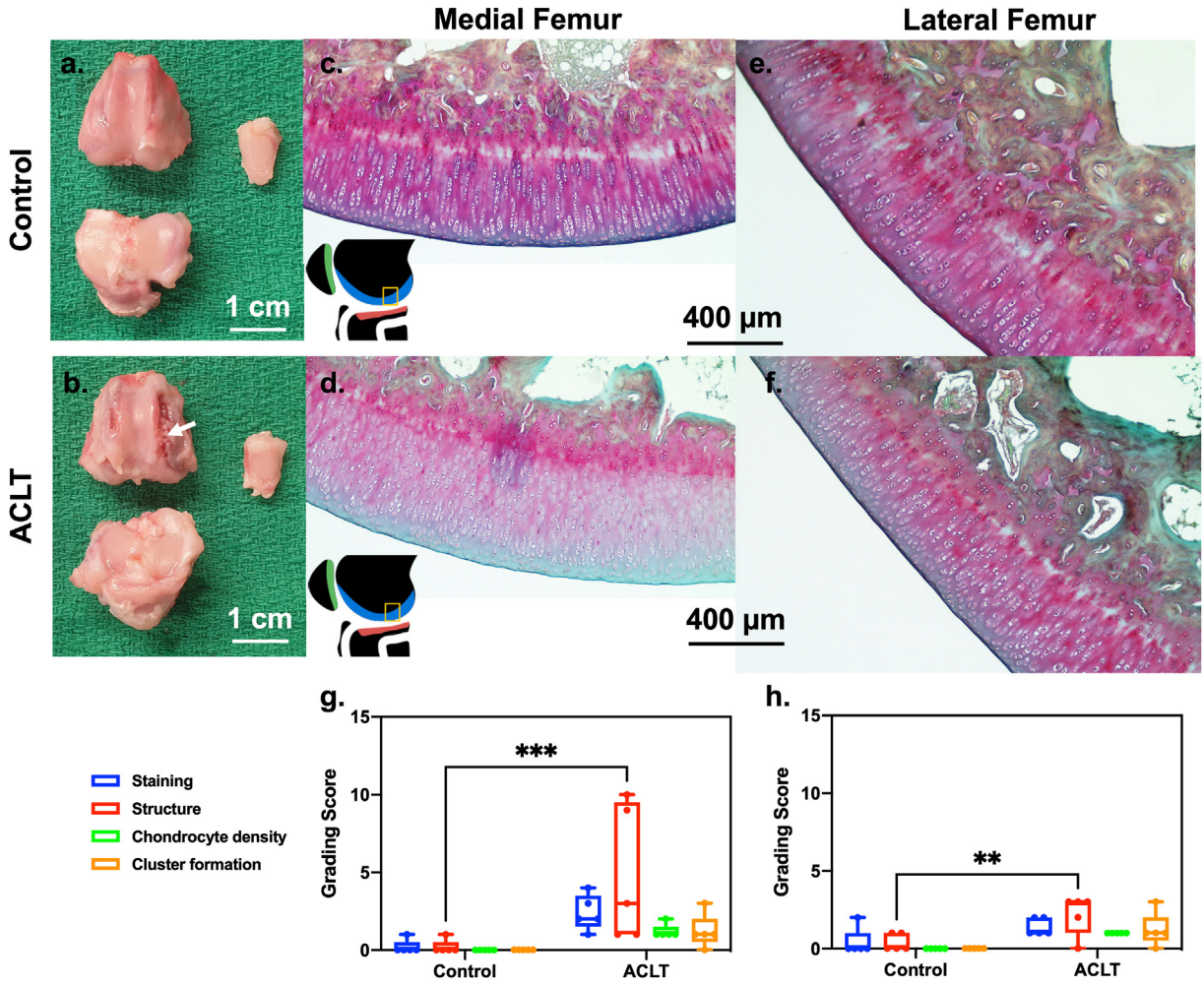

Fig. 5. Macroscopic photos of *ex vivo* gross specimens and histological microscopy demonstrate cartilage degradation due to ACLT. *Ex vivo* specimen of the femur, tibia, and patella of (a.) control knee vs. (b.) ACLT group demonstrates ulceration in the ACLT knee (white arrow) which is absent in the control knee. Representative photomicrographs of histologic specimens (Safranin O, fast green staining; original magnification, x20) show uniformly distributed cartilage cells and strong staining intensity in healthy (c.) medial and (e.) lateral femoral cartilage, whereas ACLT (d.) medial and (f.) lateral femoral cartilage were characterized by gradual gathering of chondrocytes and reduced staining intensity, indicating chondrocyte loss/apoptosis and decreased GAG content. Grading scores (n = 5 per group) for (g.) medial (***p = 0.0005) and (h.) lateral (**p = 0.0019) femoral cartilage performed using the histochemical/histological grading system outlined by Laverty et al. [38]. (For interpretation of the references to color in this figure legend, the reader is referred to the Web version of this article.)

compartment and to a lesser degree in the tibia and patella (Fig. 6). 3D renderings were generated after ACLT and control bones image registration to quantify osteophyte volumes. Osteophytes were visible in all 5 (100%) of the ACLT samples. No osteophyte formation was detected in the contralateral control knees. Lateral and medial differences were quantified as a volumetric shape difference between ACLT and control bones, caused by osteophytes. Total osteophyte volume of both medial and lateral compartments determined from μCT analysis are as follows: femoral osteophyte volume, 94.53 ± 44.08 mm^3; tibial osteophyte volume, 29.35 ± 13.79 mm^3; patellar osteophyte volume, 3.84 ± 0.92 mm^3.

There was a significant difference between the medial (74.53 ± 25.22 mm^3) and lateral (20.00 ± 7.23 mm^3) osteophyte volume in the femurs (p = 0.03). Results were normalized by calculating the ratio between total osteophyte volume and ACLT epiphysis volume in each sample. No significant difference in femur-tibial or tibial-patellar osteophyte ratio was found, although a statistically significant difference was seen between the femur and patella (p = 0.048), indicating that osteophyte formation occurs in larger bone structures of analyzed epiphysis.

4. Discussion

To date, most investigations that present quantitative information regarding articular cartilage in PTOA have focused on morphology, thickness, and volume, but these parameters have limitations [39]. For example, there is significant baseline variability in cartilage volume as a function of bone or patient size [40]. Additionally, PTOA involves important modifications in the biochemical composition of the macromolecular network of articular cartilage which is the principal source of tensile and shear strength [41]. Loss of GAG content represents the earliest stage of cartilage degeneration while the collagen content remains intact, leaving quantitative morphologic metrics unchanged and therefore unsuitable for early PTOA diagnosis [42].

Here, we have demonstrated the feasibility of dGEMRIC combined with UHF-MRI in a rabbit PTOA model using a commercially available 7 T human MRI scanner and knee coil to detect biochemical changes that precede morphologic cartilage degeneration. Surgical ACLTs were performed unilaterally to induce PTOA in female rabbits and were followed by a progressive decline in the dGEMRIC index in the medial compartment of the injured knee reaching statistical significance as early as 7- and 10-weeks post-surgery with 35% and 39% decrease compared to baseline (p = 0.009, p = 0.006), respectively. This indicates that significant GAG content reduction begins very early post injury, suggesting the need for early intervention to prevent or minimize PTOA. Site-specific PTOA was subsequently confirmed by demonstrating medial

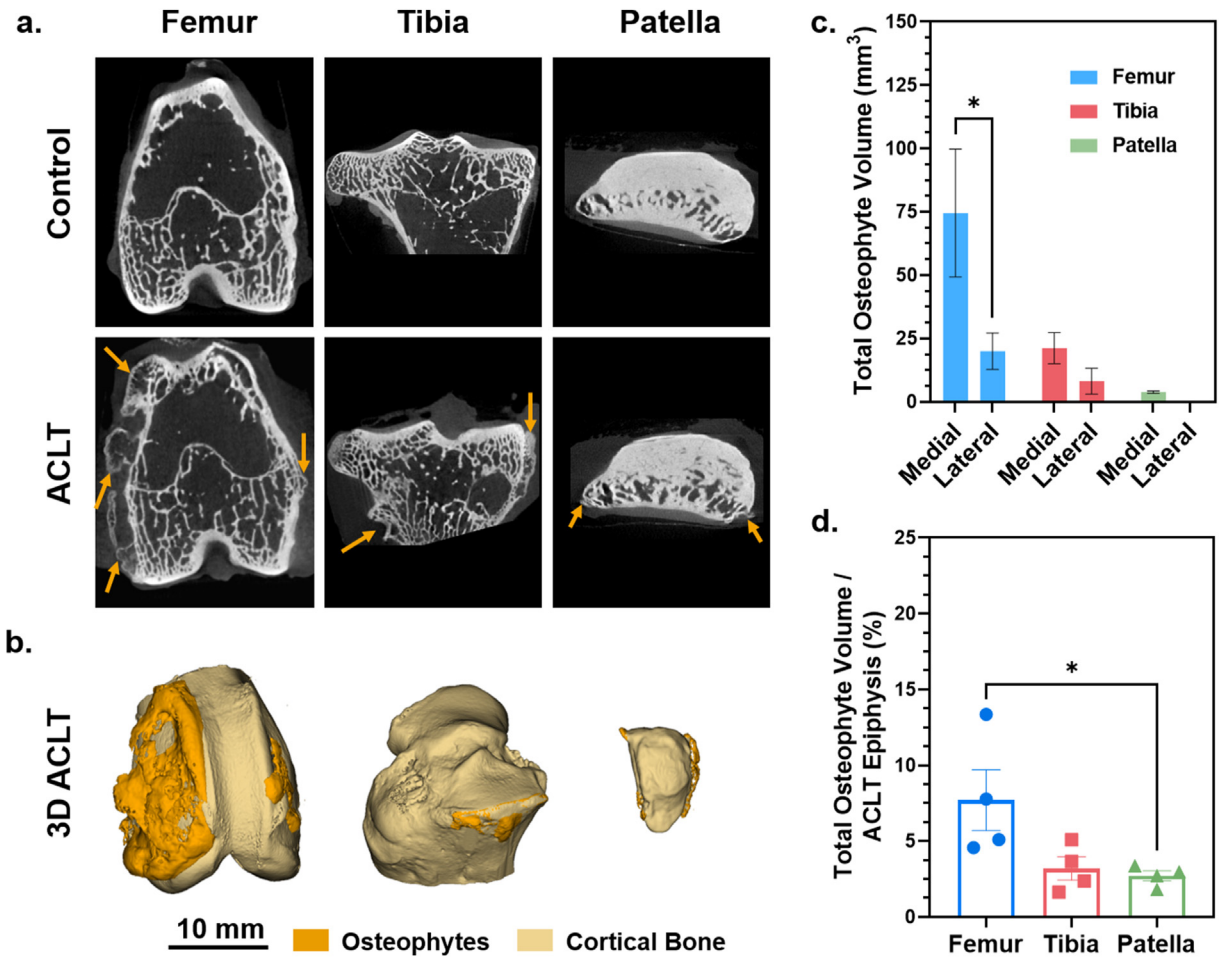

Fig. 6. (a.) Coronal μCT slices of an *ex vivo* femur, tibia, and patella in a control and ACLT joint demonstrating osteophyte development. (b.) μCT images demonstrate osteophytes at the ACLT joint margins in the medial compartment of the femur, tibia, and patella (arrows) which are absent in the contralateral controls. 3D volume renderings were generated. To ensure consistency in the volumetric analysis of subchondral bone and to allow for subsequent shape comparisons between pairs of femurs, tibiae, and patellar bones, we applied a 3D image registration to the μCT scans, co-aligning ACLT bones to their contralateral controls. Osteophyte volumes are rendered in dark yellow along the medial and lateral regions. Image subtraction was applied to determine the volumetric differences between pairs of femurs, tibiae, and patellae. Lateral and medial differences were quantified as a volumetric shape difference between the ACLT and control bones, caused by osteophytes. (c.) Total volume of quantified osteophytes as well as (d.) normalized ratio between total osteophyte volume and ACLT epiphysis volume. (For interpretation of the references to color in this figure legend, the reader is referred to the Web version of this article.)

compartment osteophytes with μCT and histopathologic confirmation of cartilage degradation. Indeed, by 10-weeks post-injury we observed histologic changes in staining (greater loss of staining in the ACLT knees), structure, density, and cluster formation, indicating multiple morphological differences.

Other studies using large animal models of ACLT have quantitatively assessed the dGEMRIC index at lower field strengths. Wei et al. [27] used an ACL injury porcine model and measured dGEMRIC index using fast spin echo sequence after Gd injection. The authors found a reduction of T1Gd in full thickness cartilage regions, while our study highlights site-specific dGEMRIC index reduction. However, Wei et al. used lower field strength (3 T) and only assessed changes for up to six weeks, while our study extends to ten weeks. Similar to this work, Laurent et al. [13] studied osteoarthritis in the rabbit knee, but the authors used a different disease model, shorter study timeline, and lower field strength. Their model was created through intraarticular injection of the proteolytic enzyme papain to reduce proteoglycan content, and images were only taken 1-h post-injection at 3 T. Because these precedent studies were both performed at lower field strength, their results may not be directly applicable at UHF-MRI, where T1 relaxivity of gadolinium is different, and imaging protocols need to be adapted. To this end, a longitudinal study conducted by Wachsmuth et al. [26] at UHF of surgically induced ACLT in a rabbit model did report visual increase of cartilage signal intensity in the medial tibial cartilage, although no quantitative dGEMRIC index was reported. In this study, we provide dGEMRIC index which quantitatively reflects depletion of GAG in the damaged cartilage indicative of PTOA.

Our evaluations of the morphologic characteristics of subchondral bone remodeling using 3D high-resolution μCT as well as histological evaluations after joint explant confirmed site-specific medial compartment degeneration induced by early PTOA, which was in agreement with the dGEMRIC data as well as previous knee biomechanics studies [43]. It is hypothesized that PTOA develops specifically in the medial compartment in early stages due to alterations in knee kinematics and contact mechanics after ACL injury resulting in increased stress on weightbearing cartilage of the medial femoral condyle [15]. Despite the fact that the loading conditions of the rabbit and human are substantially different, previous data reported that after surgical ACLT in rabbits, the medial tibial plateau undergoes extensive remodeling with prominent osteophytes at the posterior lip of the medial tibial condyle [44]. In addition, the dynamic module derived from sinusoidal tests was significantly smaller in the medial compartment of the cartilage in ACLT rabbits compared to controls [45].

There were several limitations to our study. First, we noted a slight

decrease in T1 in the medial compartment of the control knee by weeks 7 and 10. However, this decline was not statistically significant, and we hypothesize that this may be attributed to altered biomechanics resulting in increased stress on the medial compartment of the uninjured knee. In fact, a similar finding was reported in a human study of ACL injury assessed with dGEMRIC index at 1.5 T [46]. Second, we noted that T1Gd was consistently lower in the injured knee than the control knee, even prior to surgery. We attribute this effect to residual field inhomogeneity, which has been observed previously using similar setups with UHF-MRI [47]. While a B1 field mapping sequence was performed for B1 field inhomogeneity correction (which has been proven to significantly reduce the variance in the estimated T1 map) [35], it is possible that residual inhomogeneities remained. Third, our T2 mapping sequence did not demonstrate a significant change between injured and control knees. Absolute T2 values are affected by both free and bound water [48], and T2 mapping of knee articular cartilage has been shown to be highly dependent not only on acquisition techniques but also calculation methods [49]. T2 mapping and T1rho in both the hip and knee in humans have been shown as biomarkers for osteoarthritis progression but this was performed at lower field strength, such as 3 T [50,51]. However, precedent studies in a large animal model of ACLT also demonstrated no significant change in T2 after 4 weeks post-surgery, similar to our results [27]. We hypothesize that Gd contrast does not affect our T2 results as we compared T2 mapping with and without contrast prior to injury and obtained T2 values for both knees within error (right $T2_{\text{without contrast}} = 12.91 \pm 9.67$ ms versus $T2_{\text{with contrast}} = 15.23 \pm 8.70$ ms and left $T2_{\text{without contrast}} = 15.72 \pm 9.21$ ms versus $T2_{\text{with contrast}} = 16.50 \pm 8.26$ ms). However, this comparison was not repeated after injury. We believe further development and standardization is needed to optimize a T2 mapping protocol for a rabbit model of PTOA at UHF-MRI. Finally, one of the main study limitations that should be addressed is the number of animals involved. Although a significant change was found in the dGEMRIC index over time, we conducted this study with a relatively small sample size ($n = 5$). This may also have affected the statistical power of our T2 measurements, where statistical significance was not achieved. Further investigations are necessary in this direction.

In conclusion, we have demonstrated the feasibility of a dGEMRIC protocol in a rabbit model at 7 T UHF-MRI for monitoring PTOA development and progression using a commercially available human whole-body 7 T MRI scanner and knee coil. We demonstrated a significant and progressive decline in dGEMRIC index in the medial compartment of the knee status post ACL transection, which was validated histologically and by μCT, which revealed osteophyte formation only in the injured knee post-mortem (total volume of femoral: 94.53 ± 44.08 mm^3; tibial: 29.35 ± 13.79 mm^3; and patellar osteophytes: 3.84 ± 0.92 mm^3) with significantly larger volumes in the medial compartment of the femur compared to lateral ($p = 0.0312$). These results encourage further investigation and validation of the dGEMRIC technique at UHF-MRI in rabbit models of PTOA. This may, for example, be of benefit in drug and therapeutic trials as well as in human studies at 7 T. Future studies and further technical developments are needed for T2 mapping protocol optimization, perhaps with larger sample sizes. In addition, future developments including deep learning-based reconstruction may further reduce scan times substantially.

Author contributions

Guarantors of integrity of entire study, all authors; study concepts/study design or data acquisition or data analysis/interpretation, all authors; manuscript drafting or manuscript revision for important intellectual content, all authors; approval of final version of submitted manuscript, all authors; agrees to ensure any questions related to the work are appropriately resolved, all authors; literature research, R.T., Y.C.B., C.S.F; experimental studies, R.T., Y.C.B., A.L.R.R., C.S.F; statistical analysis, R.T.; Obtaining of funding, B.K.W., C.S.F.; and manuscript editing, R.T., Y.C.B., D.D., J.S.L., J.D.H., B.K.W., N.G., C.S.F.

Funding sources

This research was supported by the Department of Orthopedics Pilot Project Initiative (B.K.W., C.S.F.) and funds from Houston Methodist Research Institute (C.S.F.).

Declaration of competing interest

The authors declare no conflict of interest. N.G. has research support from Siemens Healthineers and has received financial compensation as speaker for GE healthcare for unrelated work.

Acknowledgments

We thank the Comparative Medicine Program at Houston Methodist Research Institute (HMRI) for their support during the *in vivo* rabbit experiment, as well as the staff of the MRI Core at the HMRI Translational Imaging Center, Dr. Xiaowei Zou from Siemens Medical Solutions for advice on use of UHF MR, Mr. Daryl Schulz from HMRI Pre-Clinical Catheterization Laboratory, the Microscopy Core, and the HMRI Research Pathology Core for their contributions.

Appendix A. Supplementary data

Supplementary data to this article can be found online at https://doi.org/10.1016/j.ocarto.2022.100259.

References

[1] A.C. Thomas, T. Hubbard-Turner, E.A. Wikstrom, R.M. Palmieri-Smith, Epidemiology of posttraumatic osteoarthritis, J. Athl. Train. 52 (6) (2017) 491–496, https://doi.org/10.4085/1062-6050-51.5.08.

[2] C.B. Little, D.J. Hunter, Post-traumatic osteoarthritis: from mouse models to clinical trials, Nat. Rev. Rheumatol. 9 (8) (2013) 485–497, https://doi.org/10.1038/nrrheum.2013.72.

[3] W.C. Kramer, K.J. Hendricks, J. Wang, Pathogenetic mechanisms of posttraumatic osteoarthritis: opportunities for early intervention, Int. J. Clin. Exp. Med. 4 (4) (2011) 285–298.

[4] D.D. Anderson, S. Chubinskaya, F. Guilak, et al., Post-traumatic osteoarthritis: improved understanding and opportunities for early intervention, J. Orthop. Res. 29 (6) (2011) 802–809, https://doi.org/10.1002/jor.21359.

[5] J. Lieberthal, N. Sambamurthy, C.R. Scanzello, Inflammation in joint injury and post-traumatic osteoarthritis, Osteoarthritis Cartilage 23 (11) (2015) 1825–1834, https://doi.org/10.1016/j.joca.2015.08.015.

[6] M.H. Jones, S.R. Oak, J.T. Andrish, et al., Predictors of radiographic osteoarthritis 2 to 3 Years after anterior cruciate ligament reconstruction: data from the MOON on-site nested cohort, Orthop. J. Sports Med. 7 (8) (2019), https://doi.org/10.1177/2325967119867085, 2325967119867085.

[7] R. Kijowski, D.G. Blankenbaker, P.T. Stanton, J.P. Fine, A.A. De Smet, Radiographic findings of osteoarthritis versus arthroscopic findings of articular cartilage degeneration in the tibiofemoral joint, Radiology 239 (3) (2006) 818–824, https://doi.org/10.1148/radiol.2393050584.

[8] B.L. Proffen, M. McElfresh, B.C. Fleming, M.M. Murray, A comparative anatomical study of the human knee and six animal species, Knee 19 (4) (2012) 493–499, https://doi.org/10.1016/j.knee.2011.07.005.

[9] D.L. Batiste, A. Kirkley, S. Laverty, L.M.F. Thain, A.R. Spouge, D.W. Holdsworth, Ex vivo characterization of articular cartilage and bone lesions in a rabbit ACL transection model of osteoarthritis using MRI and micro-CT, Osteoarthritis Cartilage 12 (12) (2004) 986–996, https://doi.org/10.1016/j.joca.2004.08.010.

[10] D. Dare, S. Rodeo, Mechanisms of post-traumatic osteoarthritis after ACL injury, Curr. Rheumatol. Rep. 16 (10) (2014) 448, https://doi.org/10.1007/s11926-014-0448-1.

[11] D. Chen, J. Shen, W. Zhao, et al., Osteoarthritis: toward a comprehensive understanding of pathological mechanism, Bone Res. 5 (2017) 16044, https://doi.org/10.1038/boneres.2016.44.

[12] J.S. Everhart, J.H. Sojka, C.C. Kaeding, A.L. Bertone, D.C. Flanigan, The ACL injury response: a collagen-based analysis, Knee 24 (3) (2017) 601–607, https://doi.org/10.1016/j.knee.2017.01.013.

[13] D. Laurent, J. Wasvary, E. O'Byrne, M. Rudin, In vivo qualitative assessments of articular cartilage in the rabbit knee with high-resolution MRI at 3 T, Magn. Reson. Med. 50 (3) (2003) 541–549, https://doi.org/10.1002/mrm.10566.

[14] A.W. Kajabi, V. Casula, S. Ojanen, et al., Multiparametric MR imaging reveals early cartilage degeneration at 2 and 8 weeks after ACL transection in a rabbit model, J. Orthop. Res. 38 (9) (2020) 1974–1986, https://doi.org/10.1002/jor.24644.

[15] L.J. Wang, N. Zeng, Z.P. Yan, J.T. Li, G.X. Ni, Post-traumatic osteoarthritis following ACL injury, Arthritis Res. Ther. 22 (1) (2020) 57, https://doi.org/10.1186/s13075-020-02156-5.

[16] S.Z.S. Sulaiman, W.M. Tan, R. Radzi, et al., Comparison of bone and articular cartilage changes in osteoarthritis: a micro-computed tomography and histological study of surgically and chemically induced osteoarthritic rabbit models, J. Orthop. Surg. 16 (1) (2021) 663, https://doi.org/10.1186/s13018-021-02781-z.
[17] A. Guermazi, H. Alizai, M.D. Crema, S. Trattnig, R.R. Regatte, F.W. Roemer, Compositional MRI techniques for evaluation of cartilage degeneration in osteoarthritis, Osteoarthritis Cartilage 23 (10) (2015) 1639–1653, https://doi.org/10.1016/j.joca.2015.05.026.
[18] F.W. Roemer, M.D. Crema, S. Trattnig, A. Guermazi, Advances in imaging of osteoarthritis and cartilage, Radiology 260 (2) (2011) 332–354, https://doi.org/10.1148/radiol.11101359.
[19] A. Gillis, M. Gray, D. Burstein, Relaxivity and diffusion of gadolinium agents in cartilage, Magn. Reson. Med. 48 (6) (2002) 1068–1071, https://doi.org/10.1002/mrm.10327.
[20] M.D. Crema, F.W. Roemer, M.D. Marra, et al., Articular cartilage in the knee: current MR imaging techniques and applications in clinical practice and research, Radiographics 31 (1) (2011) 37–61, https://doi.org/10.1148/rg.311105084.
[21] T.S. Ali, I. Prasadam, Y. Xiao, K.I. Momot, Progression of Post-Traumatic Osteoarthritis in rat meniscectomy models: comprehensive monitoring using MRI, Sci. Rep. 8 (1) (2018) 6861, https://doi.org/10.1038/s41598-018-25186-1.
[22] Y. Kang, J.Y. Choi, H.J. Yoo, S.H. Hong, H.S. Kang, Delayed gadolinium-enhanced MR imaging of cartilage: a comparative analysis of different gadolinium-based contrast agents in an ex vivo porcine model, Radiology 282 (3) (2017) 734–742, https://doi.org/10.1148/radiol.2016160367.
[23] C. Jaimes, N.A. Chauvin, J. Delgado, D. Jaramillo, MR imaging of normal epiphyseal development and common epiphyseal disorders, Radiographics 34 (2) (2014) 449–471, https://doi.org/10.1148/rg.342135070.
[24] P. Peterson, C.J. Tiderius, E. Olsson, B. Lundin, L.E. Olsson, J. Svensson, Knee dGEMRIC at 7 T: comparison against 1.5 T and evaluation of T1-mapping methods, BMC Muscoskel. Disord. 19 (1) (2018) 149, https://doi.org/10.1186/s12891-018-2071-1.
[25] G.H. Welsch, T.C. Mamisch, T. Hughes, et al., In vivo biochemical 7.0 tesla magnetic resonance: preliminary results of dGEMRIC, zonal T2, and T2* mapping of articular cartilage, Invest. Radiol. 43 (9) (2008) 619–626, https://doi.org/10.1097/RLI.0b013e31817e9122.
[26] L. Wachsmuth, R. Keiffer, H.P. Juretschke, R.X. Raiss, N. Kimmig, E. Lindhorst, In vivo contrast-enhanced micro MR-imaging of experimental osteoarthritis in the rabbit knee joint at 7.1T1, Osteoarthritis Cartilage 11 (12) (2003) 891–902, https://doi.org/10.1016/j.joca.2003.08.008.
[27] B. Wei, M. Zong, C. Yan, et al., Use of quantitative MRI for the detection of progressive cartilage degeneration in a mini-pig model of osteoarthritis caused by anterior cruciate ligament transection, J. Magn. Reson. Imag. 42 (4) (2015) 1032–1038, https://doi.org/10.1002/jmri.24862.
[28] J.T. Sieker, B.L. Proffen, K.A. Waller, et al., Transcriptional profiling of articular cartilage in a porcine model of early post-traumatic osteoarthritis, J. Orthop. Res. 36 (1) (2018) 318–329, https://doi.org/10.1002/jor.23644.
[29] P. Vavken, B.C. Fleming, A.N. Mastrangelo, J.T. Machan, M.M. Murray, Biomechanical outcomes after bioenhanced anterior cruciate ligament repair and anterior cruciate ligament reconstruction are equal in a porcine model, Arthroscopy 28 (5) (2012) 672–680, https://doi.org/10.1016/j.arthro.2011.10.008.
[30] A. Schafrum Macedo, C. Cezaretti Feitosa, F. Yoiti Kitamura Kawamoto, et al., Animal modeling in bone research—should we follow the White Rabbit? Anim. Models Exp. Med. 2 (3) (2019) 162–168, https://doi.org/10.1002/ame2.12083.
[31] N. Voskanian, ACL Injury prevention in female athletes: review of the literature and practical considerations in implementing an ACL prevention program, Curr. Rev. Musculoskelet. Med. 6 (2) (2013) 158–163, https://doi.org/10.1007/s12178-013-9158-y.
[32] S.L. Hame, R.A. Alexander, Knee osteoarthritis in women, Curr. Rev. Musculoskelet. Med. 6 (2) (2013) 182–187, https://doi.org/10.1007/s12178-013-9164-0.
[33] U. Sigurdsson, G. Müller, C. Siversson, et al., Delayed gadolinium-enhanced MRI of meniscus (dGEMRIM) and cartilage (dGEMRIC) in healthy knees and in knees with different stages of meniscus pathology, BMC Muscoskel. Disord. 17 (1) (2016) 406, https://doi.org/10.1186/s12891-016-1244-z.
[34] H.J. Braun, G.E. Gold, Advanced MRI of articular cartilage, Imag. Med. 3 (5) (2011) 541–555, https://doi.org/10.2217/iim.11.43.
[35] Y. Lee, M.F. Callaghan, Z. Nagy, Analysis of the precision of variable flip angle T1 mapping with emphasis on the noise propagated from RF transmit field maps, Front. Neurosci. (2017), https://doi.org/10.3389/fnins.2017.00106, 0.
[36] Y. Shen, F.L. Goerner, C. Snyder, et al., T1 relaxivities of gadolinium-based magnetic resonance contrast agents in human whole blood at 1.5, 3, and 7 T, Invest. Radiol. 50 (5) (2015) 330–338, https://doi.org/10.1097/RLI.0000000000000132.
[37] D. Milford, N. Rosbach, M. Bendszus, S. Heiland, Mono-exponential fitting in T2-relaxometry: relevance of offset and first echo, PLoS One 10 (12) (2015), e0145255, https://doi.org/10.1371/journal.pone.0145255.
[38] S. Laverty, C.A. Girard, J.M. Williams, E.B. Hunziker, K.P.H. Pritzker, The OARSI histopathology initiative – recommendations for histological assessments of osteoarthritis in the rabbit, Osteoarthritis Cartilage 18 (2010) S53–S65, https://doi.org/10.1016/j.joca.2010.05.029.
[39] F. Eckstein, W. Wirth, Quantitative cartilage imaging in knee osteoarthritis, Arthritis 2011 (2011) 475684, https://doi.org/10.1155/2011/475684.
[40] A.J. Teichtahl, Y. Wang, S. Heritier, et al., The interaction between physical activity and amount of baseline knee cartilage, Rheumatology 55 (7) (2016) 1277–1284, https://doi.org/10.1093/rheumatology/kew045.
[41] P.A. Rivers, M.P. Rosenwasser, V.C. Mow, et al., Osteoarthritic changes in the biochemical composition of thumb carpometacarpal joint cartilage and correlation with biomechanical properties, J. Hand Surg. Am. 25 (5) (2000) 889–898, https://doi.org/10.1053/jhsu.2000.16358.
[42] E.H.G. Oei, J. van Tiel, W.H. Robinson, G.E. Gold, Quantitative radiologic imaging techniques for articular cartilage composition: toward early diagnosis and development of disease-modifying therapeutics for osteoarthritis, Arthritis Care Res. 66 (8) (2014) 1129–1141, https://doi.org/10.1002/acr.22316.
[43] S.P. Ojanen, M.A.J. Finnilä, Mäkelä Jta, et al., Anterior cruciate ligament transection of rabbits alters composition, structure and biomechanics of articular cartilage and chondrocyte deformation 2 weeks post-surgery in a site-specific manner, J. Biomech. 98 (2020) 109450, https://doi.org/10.1016/j.jbiomech.2019.109450.
[44] C. Boulocher, M.E. Duclos, F. Arnault, et al., Knee joint ultrasonography of the ACLT rabbit experimental model of osteoarthritis: relevance and effectiveness in detecting meniscal lesions, Osteoarthritis Cartilage 16 (4) (2008) 470–479, https://doi.org/10.1016/j.joca.2007.07.012.
[45] C. Florea, M.k. h. Malo, J. Rautiainen, et al., Alterations in the properties of rabbit articular cartilage and underlying bone at four weeks after anterior cruciate ligament transection, Orthopaedic Proc. 96-B (SUPP_11) (2014), https://doi.org/10.1302/1358-992X.96BSUPP_11.CORS2013-095, 95-95.
[46] B.C. Fleming, H.L. Oksendahl, W.A. Mehan, et al., Delayed gadolinium-enhanced MR imaging of cartilage (dGEMRIC) following ACL injury, Osteoarthritis Cartilage 18 (5) (2010) 662–667, https://doi.org/10.1016/j.joca.2010.01.009.
[47] M.A. Dieringer, M. Deimling, D. Santoro, et al., Rapid parametric mapping of the longitudinal relaxation time T1 using two-dimensional variable flip angle magnetic resonance imaging at 1.5 tesla, 3 tesla, and 7 tesla, PLoS One 9 (3) (2014), e91318, https://doi.org/10.1371/journal.pone.0091318.
[48] S. Abbasi-Rad, H. Saligheh Rad, Quantification of human cortical bone bound and free water in vivo with ultrashort echo time MR imaging: a model-based approach, Radiology 283 (3) (2017) 862–872, https://doi.org/10.1148/radiol.2016160780.
[49] M. Mars, M. Chelli, Z. Tbini, F. Ladeb, S. Gharbi, MRI T2 mapping of knee articular cartilage using different acquisition sequences and calculation methods at 1.5 tesla, Med. Princ. Pract. 27 (5) (2018) 443–450, https://doi.org/10.1159/000490796.
[50] A.P. Prasad, L. Nardo, J. Schooler, G.B. Joseph, T.M. Link, T1ρ and T2 relaxation times predict progression of knee osteoarthritis, Osteoarthritis Cartilage 21 (1) (2013) 69–76, https://doi.org/10.1016/j.joca.2012.09.011.
[51] M.C. Gallo, C. Wyatt, V. Pedoia, et al., T1ρ and T2 relaxation times are associated with progression of hip osteoarthritis, Osteoarthritis Cartilage 24 (8) (2016) 1399–1407, https://doi.org/10.1016/j.joca.2016.03.005.